Journal of the Serbian Chemical Society
JSCS-info@shd.org.rs • www.shd.org.rs/JSCS
J. Serb. Chem. Soc. *87* (11) 1285–1296 (2022)
JSCS–5594
Original scientific paper
Published 20 October 2022

Nanoemulsification synthesis route for obtaining highly efficient Ag_3PO_4 photocatalytic nanomaterial

MARIJA PREKAJSKI ĐORĐEVIĆ[1]*, ALEKSANDRA ZARUBICA[2], ANA KALIJADIS[1], BILJANA BABIĆ[3], SVETLANA BUTULIJA[1], JELENA MALETAŠKIĆ[1] and BRANKO MATOVIĆ[1]

[1]*Department of Materials Science, "Vinča" Institute of Nuclear Science – National Institute of the Republic of Serbia, University of Belgrade, PO Box 522, 11001 Belgrade, Serbia,* [2]*Department of Chemistry, Faculty of Science and Mathematics, University of Niš, Višegradska 33, 18000 Niš, Serbia and* [2]*Institute of Physics Belgrade, University of Belgrade, Pregrevica 118, 11000, Belgrade, Serbia*

(Received 3 November 2021, revised 27 June, accepted 28 June 2022)

Abstract: Nanoemulsion technique based on Ouzo effect was applied for the fast and simple synthesis of Ag_3PO_4 at room temperature. X-ray powder diffraction analysis and Raman spectroscopy reviled that synthesized powder was single-phase. Using scanning electron microscopy analysis, it was found that the synthesized Ag_3PO_4 particles were near-spherical shape with an average diameter of 100 nm. The high value for the specific surface area of obtained powder was measured by Brunauer–Emmet–Teller method. Finally, the Ag_3PO_4 product was used as a photocatalyst for the photodegradation of crystal violet dye in an aqueous solution. Nanoemulsion strategy procedure provides a simple pathway to obtain a highly efficient single-phase Ag_3PO_4 photocatalyst.

Keywords: XRD; Raman; BET; BJH; photodegradation.

INTRODUCTION

The assembly of organic dyes and unsafe wastage from industries produce environmental problems, such as air and water pollution. Many techniques have been developed for the removal of organic dyes from wastewater, including adsorption, photocatalysis, anaerobic treatment, membrane filtration, chemical oxidation, *etc.*[1–3] One of the most promising technologies to address the issues of environmental pollution is the direct use of sun light energy.[4] Among them, semiconductors based photocatalyst used for treating wastewater and organic dye pollutants under ultraviolet (UV) and visible (Vis) light irradiation are especially interesting due to their high efficiency, destruction ability, and availability. How-

* Corresponding author. E-mail: prekajski@vin.bg.ac.rs
https://doi.org/10.2298/JSC211103055P

ever, some photocatalysts can only be excited by UV light. It is well-known that the UV region occupies only approximately 4% of the entire solar spectrum, while 43 % of the energy belongs to Vis light. Therefore, the development of novel photocatalysts, particularly Vis light-responsive catalysts, are necessary for the efficient utilization of solar energy in photocatalysis, and for these reasons, there is an increasing interest in pursuing an ideal photocatalyst to effectively utilize the Vis light of solar radiation.

Among many photocatalyst materials, silver orthophosphate (Ag_3PO_4) has attracted considerable attention since Yi *et al.* discovered it in 2010.[5–7] In the last few years, many efforts have been devoted to further improving and optimizing the photocatalytic activity and stability of Ag_3PO_4. It was found that photodegradation activity and applications of this phosphate are profoundly dependent on its size, morphology, and specific surface area, and thus the photocatalytic efficiency of Ag_3PO_4 can be improved by controlling the morphology and crystal structure of the material. Therefore, great attention has been paid on devising appropriate synthesis processes for obtaining efficient Ag_3PO_4 catalysts. Many methods have been evolved that as result produces various morphologies and sizes of Ag_3PO_4, which include spheres,[8–10] dodecahedrons,[11] tetrahedrons,[11,12] cubes,[13,14] mesocrystals,[11] concave trisoctahedron,[15] gyro shape,[16] *etc*. However, their practical application is restricted because of several limiting factors, for instance, the tedious work involved in the preparation and removal of the surfactants and/or templates. Particularly, the templates or surfactants are not eco-friendly and not suitable for large-scale production.[17] Hence, it is still an important research field to find an economic and green method for controlling the size and morphology of Ag_3PO_4. Although a large number of modifications have been adopted in the synthesis techniques, the optimum synthesis conditions are still required.

In this contribution, the presented work demonstrates the successful synthesis of Ag_3PO_4 *via* an effortless and very efficient nanoemulsion synthesis method, based on the Ouzo effect. Nanoemulsions represent a special class of liquid disperse systems, with droplet diameters smaller than 100 nm.[18] Spontaneous emulsification occurs when a strongly hydrophobic oil is dissolved in a water-miscible solvent. This effect is nanoemulsification and it is usually called the Ouzo effect[19,20] where the Ouzo is a liquor that consists of anise oil dispersed in ethanol. When water is added to the Ouzo, the dissolved anise oil spontaneously nucleates into many small droplets, without the help of a surfactant. These small droplets scatter light causing the sample to appear milky white. The Ouzo effect offers the possibility of obtaining a pure nanopowder, without using any surfactants or templates, because emulsification occurs almost simultaneously in the entire volume.[21]

X-Ray powder diffraction (XRD) accompanied with the Rietveld refinement procedure enabled the crystallite size, structure and phase composition of a synthesized sample to be explored. Raman spectroscopy was used in order to confirms the composition purity of the obtained sample. The morphological properties were studied by field emission scanning electron microscopy (FE-SEM) and Brunauer–Emmett–Teller (BET) measurements. The pore size distribution (PSD) was estimated by applying the Barett–Joyner–Halenda (BJH) method. The photocatalytic activity of as-prepared Ag_3PO_4 product was investigated by photodegradation of crystal violet (CV) dye in an aqueous solution. A simple procedure for the synthesis of the effective photocatalyst was demonstrated. According to the authors' knowledge, this method was used for the very first time for the synthesis of Ag_3PO_4 nanomaterial.

EXPERIMENTAL

Ag_3PO_4 nanoparticles were synthesized using analytical grade $AgNO_3$ (Riedel-de Haën, 99 % purity) and $(NH_4)_2HPO_4$ (Riedel-de Haën, 99 % purity). Analytical grade acetone was the solvent used for making the nanoemulsion. For the synthesis, 3/100 mole of $AgNO_3$ was desolved in 0.05 dm^3 of acetone and then mixed with 1/100 mol of $(NH_4)_2HPO_4$ which was desolved in 0.05 dm^3 of water (the ratio of acetone and aqueous solution phases in nanoemulsion was 1:1). The pH in the aqueous $(NH_4)_2HPO_4$ solution was adjusted to 11 with sodium hydroxide (1 M) prior to mixing. The mixed solutions were stirred for 5 min using a magnetic stirrer. No surfactant was used in any of the synthesis processes. A nanoemulsion (milky white, almost transparent liquid) was obtained that was immediately centrifuged to avoid particle agglomeration and then washed three times using ultra-pure deionized water. Finally, the slurry of nanoprecipitates was dried in an oven at 50 °C, for 12 h, in order to obtain a dry powder.

The phase purity and crystallinity of the produced powder were examined using X-ray diffraction (Raguku Ultima IV, Japan). The X-ray beam was nickel-filtered CuKα_1 radiation (λ = 0.1540 nm, operating at 40 kV and 40 mA). The XRD data were collected at 2θ from 15 to 80 ° at a scanning rate of 2 °min^{-1}. Phase analysis was realized using PDXL2 software (version 2.0.3.0),[22] with referece to the patterns of the American Mineralogist Crystal Structure Database (AMCSD).[23] Calculation of the average crystallite size (D_{hkl}) was performed using the Scherrer formula, Eq. (1):[24]

$$D_{hkl} = \frac{0.9\lambda}{\beta \cos\theta} \quad (1)$$

where λ is the wavelength of the X-rays, θ is the diffraction angle, β is the corrected half-width for instrumental broadening $\beta = (\beta_m - \beta_s)$, β_m is the observed half-width and β_s is the half-width of the standard CeO_2 sample.

The specific surface area and the pore size distribution of Ag_3PO_4 were analyzed using Surfer (Thermo Fisher Scientific, USA). The PSD was estimated using the BJH method[25] to the desorption branch of isotherms and mesopore surface, and the micropore volume were estimated using the α_s-plot method.[26]

The morphology of the dried nanoprecipitates was characterized by a Hitachi S-4800 field emission gun scanning electron microscope, with electron energies of 20 kV in high vacuum. The samples used for FE-SEM characterization were coated with 5 nm thin layer of

Au/Pd using a standard sputtering technique. The results from FE-SEM measurements showed a sample area of 2.5 μm×2.5 μm (275,000× magnification).

The photocatalytic ability of the synthesized Ag_3PO_4 nanomaterial was studied using the degradation of the organic dye crystal violet as a test. The examination the photodegradation of the cationic dye CV was chosen because in all literature data the photodegradation of this dye by Ag_3PO_4. as a photocatalyst is the least researched. Vis irradiation was applied in order to evaluate the photocatalytic activity of the Ag_3PO_4 photocatalyst. The light source was 4 Vis tungsten–halogen lumps, every with a power of 60 W. A quartz cell was used for the photocatalytic degradation test. The reaction was maintained at ambient temperature. The acidity of the solutions was not additionally adjusted, and pH values were in the range from 6.7 to 7.0. In a typical experiment, aqueous suspensions of the dye (initial concentration 500 μmol dm^{-3}) and 50 mg of the synthesized Ag_3PO_4 photocatalyst powder were placed in a beaker. The volume of the test solution (the CV colour solution) was $V = 0.05$ dm^3. Prior to irradiation, the suspension was magnetically stirred in the dark for 1 h to ensure the establishment of the adsorption/desorption equilibrium. The suspension was kept under constant air-equilibrated conditions. In addition, the same experiment was reperformed in a combination of UV + Vis irradiation, using 4 UV low-pressure Hg vapor lamps, each with power 28 W, and 4 Vis tungsten–halogen lumps, each with power 60 W.

RESULTS AND DISCUSSION

Phase structure and morphology of the porous nanospheres

The crystallinity and phase purity of the obtained product was first examined by X-ray diffraction. The XRD pattern of the as-synthesized samples (Fig. 1) revealed that the Ag_3PO_4 phase was already forming at room temperature. The synthesized powder is single-phase and all the diffraction peaks can be well indexed to cubic Ag_3PO_4 (space group *P*-43*n*), which is in accordance with the standard data AMCSD Card No.: 0017250.[23] There were no other characteristic peaks of impurities or secondary phases. The diffraction peaks were broadened that indicates the presence of small crystallite (nanocrystals) in the sample. According to the calculation based on the Scherrer Equation, the crystallite size of as synthesized samples was about 4 nm (Table I). The calculated cell parameters were $a = b = c = 0.6017208(3)$ nm. These results are in good correlation with literature data.[27,28]

The inset in Fig. 1 represents the crystal structure of Ag_3PO_4 modeled using Vesta© software version 3.3.2.[29] It depicts the cubic structure of Ag_3PO_4, in which six Ag atoms occupy only the 6*d* Wyckoff position and have 4-fold coordination by four O atoms resulting in tetrahedral [AgO_4]; the P atoms are each in [PO_4] tetrahedra, while the O atoms possess 4-fold coordination surrounded by three Ag atoms and one P atom. The isolated and regular [PO_4] tetrahedra construct a body-centered cubic lattice structure. In this modeled structure, the Ag and P atoms are coordinated with four O atoms, resulting in tetrahedral [AgO_4] and [PO_4] clusters. Each [PO_4] cluster has in its vicinity three [AgO_4] agglomerates bound by O atoms. The existence of two binding angles (α and β) indicated that

the [AgO_4] agglomerates are highly distorted in the network, because of the inductive effect caused by the high electronegativity of the clusters.[30]

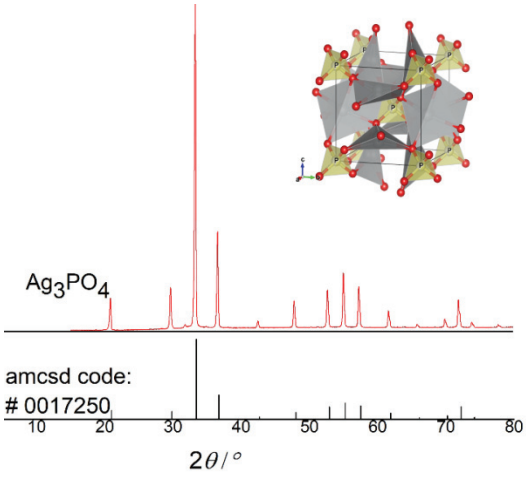

Fig. 1. XRD pattern of the synthesized Ag_3PO_4. Inset: Unit-cell structure showing the polyhedron configuration of the cubic Ag_3PO_4. Red, yellow, and grey spheres represent O, P, and Ag atoms/ /polyhedrons, respectively.

TABLE I. Calculated crystallographic parameters after refinement using PDXL2 software of the synthesized Ag_3PO_4 crystal structure

Atom	Wickoff position	*x*	*y*	*z*	Position occupation
Ag	12*h*	0.22419	0	0.5	1.5
P	2*a*	0	0	0	0.5
O	8*e*	0.1467	0.1467	0.1467	2.5
a / nm	0.6017208(3)				

Raman analysis

Further, Raman spectroscopic analysis was performed to confirm the presence of Ag_3PO_4 single phase. The Raman spectra of an as-synthesized Ag_3PO_4 sample is displayed in Fig. 2. According to literature data,[30] Ag_3PO_4 presents a

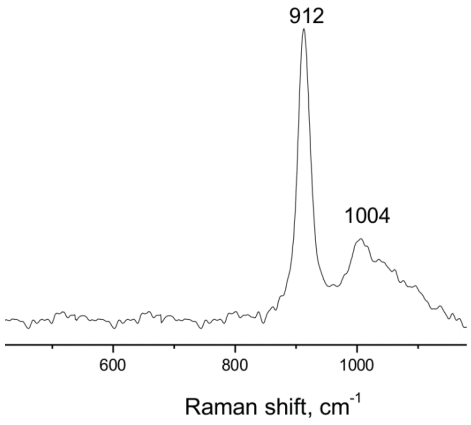

Fig. 2. Raman spectra of an as-synthesized Ag_3PO_4 sample.

total of 18 Raman-active modes. However, in this work, only two Raman-active modes were identified, both related to the PO_4^{3-} clusters. The strong and sharp absorption peak centered at about 912 cm^{-1} is attributed to the PO_4^{3-} symmetric stretching vibration of O–P–O bonds.[31] A small and broad peak at 1004 cm^{-1} is attributed to the PO_4^{3-} asymmetric stretching vibrations of the same bonds.[32] The Raman spectra confirmed the formation of single-phase Ag_3PO_4.

Morphology characterization

Further investigation was performed by FE-SEM technologies to characterize the morphology and crystal structure of the as-obtained Ag_3PO_4 nanomaterial. FE-SEM micrographs of the as-synthesized Ag_3PO_4 powder are shown in Fig. 3, particles with near-spherical shapes with an average diameter of 100–200 nm could be observed. Their morphology also resembles platelets. However, higher magnification (Fig. 3b) revealed that the particles are more likely irregular-shaped spheres. Some particle aggregation also occurs. The formation of spherical Ag_3PO_4 nanoparticles is due to the Ouzo effect, which occurs in the present synthesis method.[33] This characteristic endows the as-prepared Ag_3PO_4 porous nanospheres with a large surface area, which could affect their physicochemical properties.

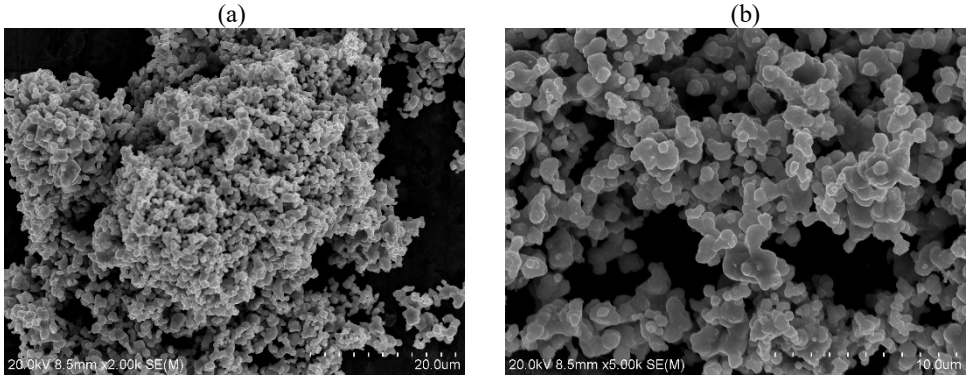

Fig. 3. FE-SEM micrographs of an as-synthesized Ag_3PO_4 sample: a) magnification 2000×; b) magnification 5000×.

Adsorption isotherms – BET experiments

Nitrogen adsorption isotherms for an Ag_3PO_4 sample, as the amount of N_2 adsorbed as a function of relative pressure at –196 °C, are shown in Fig. 4. It could be seen from the analysis that the adsorption–desorption hysteresis loop of the sample can be classified as Type IV,[34] which is associated with mesoporous materials (Fig. 4). The shape of the hysteresis loop is of type H3. Isotherms revealing type H3 hysteresis do not exhibit any limiting adsorption at high P/P_0, which is observed with non-rigid aggregates of plate-like particles giving rise to

slit-shaped pores.[35] Specific surface areas calculated by the BET equation, S_{BET}, are listed in Table II. The S_{BET} value is 42 m^2 g^{-1}. The pore size distribution, as determined with the BJH method, is shown in Fig. 5. The sample is micro- and mesoporous with one peak pore radius at 2.0 nm. The median pore radius (r_{med}) is 2.9 nm (Table II).

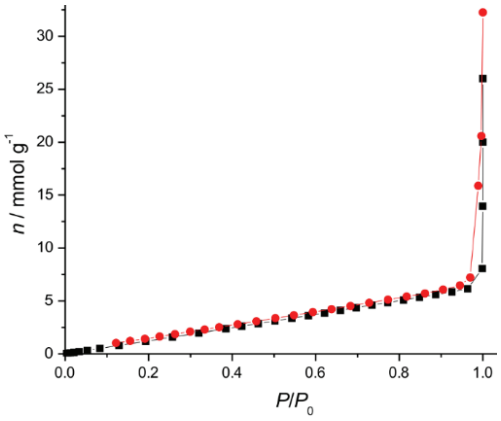

Fig. 4. Nitrogen adsorption isotherms of Ag_3PO_4. Black square symbols – adsorption, red circle symbols – desorption.

TABLE II. Porous properties of the synthesized Ag_3PO_4 nanomaterial

S_{BET} / m^2 g^{-1}	S_{meso} / m^2 g^{-1}	S_{mic} / m^2 g^{-1}	V_{meso} / dm^3 g^{-1}	V_{mic} / dm^3 g^{-1}	r_{med} / nm
42	24	18	3.2×10^{-5}	2.1×10^{-5}	2.9

The α_s-plot, obtained based on the standard nitrogen adsorption isotherm. The straight line in the medium α_s-plot region gives a mesoporous surface area including the contribution of the external surface, S_{meso}, determined by its slope, and the micropore volume, V_{mic}, is given by the intercept. The calculated porosity parameters (S_{meso}, S_{mic}, V_{meso}, V_{mic}) are given in Table II. An α_s-plot analysis confirmed that the sample was micro- and mesoporous.

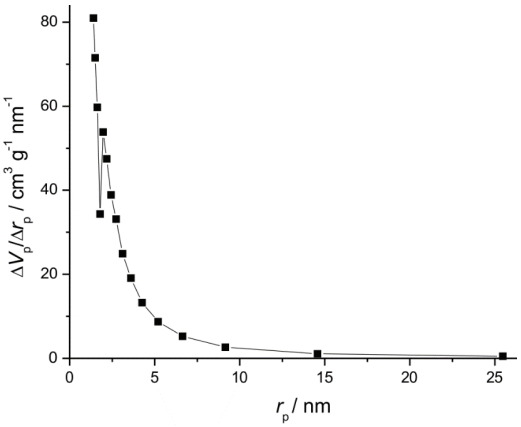

Fig. 5. Pore size distribution of Ag_3PO_4.

The specific surface area of a photocatalyst is a major parameter to measure the characteristics of the material, and its size has a great impact on its photocatalytic properties. It was shown that the specific surface areas of samples produced by the simple nanoemulsion synthesis method have larger specific surface areas than the products of other methods. For example, starting from the same components, but using the precipitation method and the ion-exchange method of synthesis, the authors obtained 8.7 and 1.2 $m^2 g^{-1}$ specific surface areas of the synthesized Ag_3PO_4, for the above-mentioned methods, respectively.[36] On the other hand, the specific surface area that was obtained using the nanoemulsion technique was 42 $m^2 g^{-1}$, which is 5 times higher than in the case of the sample obtained by the precipitation method and even 35 times higher than the specific surface area obtained in samples synthesized by the ion-exchange method. In addition, the particle size for the precipitation method is mainly centered on 0.3––0.4 μm, while the ion-exchange method predominantly ranges from 6 to 10 μm. In the present work, the particle size was the same as the crystallite size (since the crystallite is not glued together into bigger agglomerated particles). This smaller size of crystallites (particles) makes a significant contribution to obtaining higher values of the specific surface area. It could be explained by a higher ratio of surface to volume of the nanomaterials. Namely, it is known that nanoparticles have a relatively larger surface area when compared to the same volume of material made up of bigger particles. As particle size decreases, the surface area per unit volume increases. Therefore, materials made of nanoparticles have a much greater surface area per unit volume ratio compared with materials made up of bigger particles. As the surface area per mass of a material increases, a greater amount of the material can come into contact with surrounding materials, thus affecting reactivity and making the material much more efficient for photodegradation of pollutant dyes.

Photocatalytic degradation of crystal violet dye

The photocatalytic activities of the as-prepared Ag_3PO_4 samples were evaluated by the degradation of the cationic crystal violet dye. First, blank experiment was performed by irradiating an aqueous solution of the dye derivates in the absence of photocatalysts and a spectrophotometic analysis of the irradiated samples did not show any measurable loss of the dye (black squares in Fig. 6) indicating that irradiation alone is not capable of degrading CV dye. The effect of Ag_3PO_4 on the removal of CV dyes was investigated and the results are presented in Fig. 6. First, the photodegradation of CV dye on the synthesized Ag_3PO_4 photocatalyst with UV + Vis irradiation was evaluated (red dots in Fig. 6) The Ag_3PO_4 photocatalyst exhibited very good photocatalytic activity for CV dye photodegradation under Vis irradiation. After Vis irradiation for 30 min, 87 % of CV had been photodegraded. The degradation kinetics suppresed slightly

when only Vis light was used (blue triangles in Fig. 6). These results show that the synthesized Ag_3PO_4 nanomaterial works as an excellent photo-catalyst.

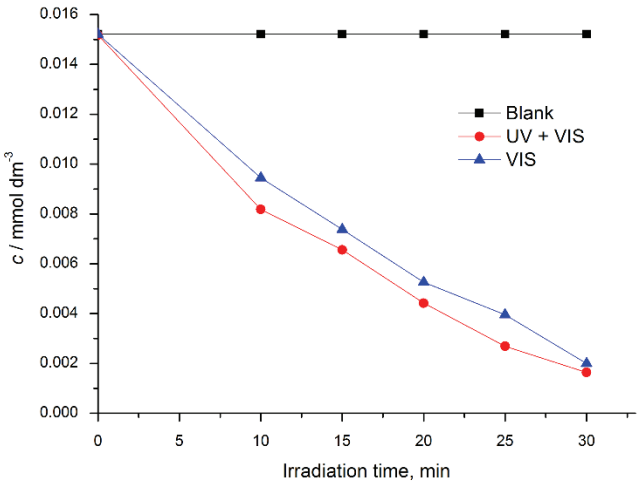

Fig. 6. Photocatalytic degradation of CV dye by Ag_3PO_4 nano-spheres sample, blank experiment (black squares), illuminated with UV + Vis (red dot) and only Vis light (blue triangle).

In the literature data, just a few research papers that deal with photodegradation of crystal violet dye using Ag_3PO_4 photocatalyst were found. Luo and co-authors[37] obtained similar results but with two-times higher concentrations of used photocatalyst. Namely, after Vis irradiation for 30 min, 93.0 % of CV dye was photodegraded, but the initial concentration of Ag_3PO_4 photocatalyst powder was 100 mg of the synthesized Ag_3PO_4 photocatalyst powder.[33] This means that a more than two-times more efficient material was obtained in the present work, which could be explained by the morphology of synthesized powders. Compared to the sample used in the present work, the Ag_3PO_4 used previously had a much larger particle size (about 4000 nm) and consequently a much smaller specific surface area (0.24 m^2 g^{-1}).[34] These are the reasons for the superior efficiency of the sample that was obtained in this using nano emulsification technique, also called the "Ouzo effect".[21]

It seems that material synthesis using the nanoemulsion method could be related to the excellent physical and chemical properties of Ag_3PO_4, *e.g.*: a higher value of the specific surface area, the presence of individual crystal phases, the small size of the crystallite/particles, *etc*.

CONCLUSIONS

A simple and low-cost nanoemulsion synthesis technique based on the Ouzo effect has been successfully used for the preparation of a Ag_3PO_4 photocatalyst. Single-phase Ag_3PO_4 was obtained at room temperature, with crystallite size

≈100 nm. The synthesized sample was micro- and meso-porous, with a specific surface area of 42 m^2 g^{-1}. The applied synthesis route gives a material with a much higher value of the specific surface area in comparison to the other synthesis methods that are described in the literature. This is very important when it comes to the application of photocatalyst. The particles were spherical in shape, with the size of about 100–200 nm. This research showed that synthesized Ag_3PO_4 photocatalyst is efficient for the photodegradation of aqueous CV dye solutions under Vis light. The present study indicates that this simple, effortless, and very efficient synthetic process provides a simple pathway to obtain a highly efficient single-phase Ag_3PO_4 photocatalyst. For these reasons, it is believed that this synthesis method could be applied for large-scale production. Plans for the future are to perform immobilization of photocatalytic material on an extremely porous filter (*e.g.*, made of Al_2O_3 ceramic) in order to allow easy extraction of photocatalytic material from wastewater.

Acknowledgements. This work was supported by the Ministry of Education, Science and Technological Development of the Republic of Serbia (Theme Number: 1702021). The authors Branko Matović and Jelena Maletaskić gratefully acknowledge the financial support from the Laboratory for Advanced Nuclear Energy, Institute of Innovative Research, Tokyo Institute of Technology, 2-12-1, Okayama, Meguro-ku, Tokyo 152-8550, as visiting professors.

ИЗВОД

СИНТЕЗА ВИСОКО ЕФИКАСНОГ Ag_3PO_4 ФОТОКАТАЛИТИЧКОГ НАНОМАТЕРИЈАЛА ПРОЦЕСОМ НАНОЕМУЛЗИФИКАЦИЈЕ

МАРИЈА ПРЕКАЈСКИ ЂОРЂЕВИЋ[1], АЛЕКСАНДРА ЗАРУБИЦА[2], АНА КАЛИЈАДИС[1], БИЉАНА БАБИЋ[3], СВЕТЛАНА БУТУЛИЈА[1], ЈЕЛЕНА МАЛЕТАШКИЋ[1] и БРАНКО МАТОВИЋ[1]

[1]Лабораторија за материјале, Институт за нуклеарне науке „Винча“ – Институт од националног значаја Републике Србије, Универзитет у Београду, поштански фах 522, 11001 Београд, [2]Департман за хемију, Природно–математички факултет Универзитета у Нишу, Вишеградска 33, 18000 Ниш и [3]Институт за физику Београд, Универзитет у Београду, Прегревица 118, 11000, Београд

Наноемулзиона метода заснована на „Ouzo ефекту“ примењена је за једноставну и брзу синтезу Ag_3PO_4 на собној температури. Анализе дифракције рендгенских дијаграма праха и Раманове спетроскопије показали су да је синтетисани прах монофазан. Методом скенирајуће електронске микроскопије утврђено је да су синтетисане честице Ag_3PO_4 сферног облика, просечног пречника 100 nm. Висока вредност специфичне површине добијеног праха мерена је Brunauer–Emmet–Teller методом. Добијени нанопрах Ag_3PO_4 коришћен је као фотокатализатор за фотодеградацију кристално љубичасте боје у воденим растворима. Резултати су показали потпуну деградацију при кратком времену зрачења. Закључује се да је метода наноемулзификације једноставан начин за добијање високо-ефикасног монофазног Ag_3PO_4 фотокатализатора.

(Примљено 3. новембра 2021, ревидирано 27. јуна, прихваћено 28. јуна 2022)

REFERENCES

1. N. Atar, A. Olgun, S. Wang, *Chem. Eng. J.* **192** (2012) 1 (https://doi.org/10.1016/j.cej.2012.03.067)

2. N. Atar, A. Olgun, S. Wang, S. Liu, *J. Chem. Eng. Data* **56** (2011) 508 (https://doi.org/10.1021/je100993m)
3. N. Atar, T. Eren, M. L. Yola, H. Karimi-Maleh, B. Demirdögena, *RSC Adv.* **5** (2015) 26402 (https://doi.org/10.1039/C5RA03735B)
4. A. Kubacka, M. Fernandez-Garcia, G. Colon, *Chem. Rev.* **112** (2012) 1555 (https://doi.org/10.1021/cr100454n)
5. Z. G. Yi, J. H. Ye, N. Kikugawa, T. Kako, S. Ouyang, H. Stuart-Williams, H. Yang, J. Cao, W. Luo, Z. Li, Y. Liu, R. L. Withers, *Nat. Mater.* **9** (2010) 559 (https://doi.org/10.1038/nmat2780)
6. G. H. Huang, Z. L. Ma, W. Q. Huang, Y. Tian,1 C. Jiao, Z. M. Yang, Z. Wan, A. Pan, *J. Nanomater.* **2013** (2013) 1 (https://doi.org/10.1155/2013/371356)
7. H. Wang, Y. S. Bai, J. T. Yang, X. Lang, J. Li, L. Guo, *Chem. Eur. J.* **18** (2012) 5524 (https://doi.org/10.1002/chem.201103189)
8. Z. M. Yang, Y. Y. Liu, L. Xu, G. F. Huang, W. Q. Huang, *Mater. Lett.* **133** (2014) 139 (https://doi.org/10.1016/j.matlet.2014.07.004)
9. X. Guan, J. Shi, L. Guo, *Int. J. Hydrogen Energy* **38** (2013) 11870 (https://doi.org/10.1016/j.ijhydene.2013.07.017)
10. Z. M. Yang, Y. Tian, G. F. Huang, W. Q. Huang, Y. Y. Liu, C. Jiao, Z. Wan, X. G. Yan, A. Pan, *Mater. Lett.* **116** (2014) 209 (https://doi.org/10.1016/j.matlet.2013.11.041)
11. P. Dong, Y. Yin, N. Xu, R. Guana, G. Hou, Y. Wang, *Mater. Res. Bull.* **60** (2014) 682 (https://doi.org/10.1016/j.materresbull.2014.09.047)
12. L. Dong, P. Wang, S. Wang, P. Lei, Y. Wang, *Mater. Lett.* **134** (2014) 158 (https://doi.org/10.1016/j.matlet.2014.07.094)
13. X. Guo, C. Chen, S. Yin, L. Huang, W. Qin, *J. Alloy. Compd.* **619** (2015) 293 (https://doi.org/10.1016/j.jallcom.2014.09.065)
14. Y. Bi, H. Hu, S. Ouyang, G. Lu, J. Cao, Jinhua Ye, *Chem. Commun.* **48** (2012) 3748 (https://doi.org/10.1039/C2CC30363A)
15. Z. Jiao, Y. Zhang, H. Yu, G. Lu, J. Yeb, Y. Bi, *Chem. Commun.* **49** (2013) 636 (https://doi.org/10.1039/C2CC37324F)
16. J. D. Wang, J. K. Liu, C. X. Luo, Y. Lu, X. H. Yang, *Cryst. Growth Des.* **13** (2013) 4837 (https://doi.org/10.1021/cg4009812)
17. S. Kumar, T. Surendar, V. Shanker, *Mater. Lett.* **123** (2014) 172 (https://doi.org/10.1016/j.matlet.2014.02.106)
18. M. Yu Koroleva, E.V. Yurtov, *Russ. Chem. Rev.* **81** (2012) 21 (https://doi.org/10.1070/RC2012v081n01ABEH004219)
19. F. Ganachaud, J. L. Katz. *Chem. Phys. Chem.* **6** (2005) 209 (https://doi.org/10.1002/cphc.200400527)
20. W. Y. Zhou, M. Wang, W. L. Cheung, B. C. Guo, D. M. Jia. *J. Mater. Sci. Mater. Med.* **19** (2008) 103 (https://doi.org/10.1007/s10856-007-3156-9)
21. M. Prekajski, M. Mirković, B. Todorović B, A. Matković, M. Marinović-Cincović, J. Luković. B. Matović, *J. Eur. Ceram. Soc.* **36** (2016) 1293 (https://doi.org/10.1016/j.jeurceramsoc.2015.11.045)
22. *PDXL Version 2.0.3.0 Integrated X-ray Powder Diffraction Software*, Rigaku Corporation, Tokyo, 2011(https://www.rigaku.com/support/software/pdxl)
23. *American Mineralogist Crystal Structure Database (AMCSD)*, (http://rruff.geo.arizona.edu/AMS/amcsd.php, accessed in August, 2021)

24. P. Scherrer, *Gött. Nachr.* **2** (1918) 98 (http://www.digizeitschriften.de/download/PPN252457811_1918/PPN252457811_1918__log15.pdf)
25. E. P. Barret, L. G. Joyner, P. P. Halenda, *J. Am. Chem. Soc.* **73** (1951) 373 (https://doi.org/10.1021/ja01145a126)
26. B. C. Lippens, B. G. Linsen, J. H. De Boer, *J. Catal.* **3** (1964) 32 (https://doi.org/10.1016/0021-9517(64)90089-2)
27. L. Helmholz, *J. Chem. Phys.* **4** (1936) 316 (https://doi.org/10.1063/1.1749847)
28. J. F. Cruz-Filho, T. M. S. Costa, M. S. Lima, L. J. Silva, R. S. Santos, L. S. Cavalcante, E. Longo, G. E. Luz Jr., *J. Photochem. Photobiol. A* **377** (2019) 14 (https://doi.org/10.1016/j.jphotochem.2019.03.031)
29. K. Momma, F. Izumi, *J. Appl. Crystallogr.* **41** (2008) 653 (https://doi.org/10.1107/S0021889808012016)
30. G. Botelho, J. C. Sczancoski, J. Andres, L. Gracia, E. Longo, *J. Phys. Chem., C* **119** (2015) 6293 (https://doi.org/10.1021/jp512111v)
31. B. Chai, J. Li, Q. Xu, *Ind. Eng. Chem. Res.* **53** (2014) 8744 (https://doi.org/10.1021/ie4041065)
32. Z. Wang, L. Yin, M. Zhang, G. Zhou, H. Fei, H. Shi, H. Dai, *J. Mater. Sci.* **49** (2014) 1585 (https://doi.org/10.1007/s10853-013-7841-4)
33. F. Ganachaud, J. L. Katz, *Chem. Phys. Chem.* **6** (2005) 209 (https://doi.org/10.1002/cphc.200400527)
34. K. S. W. Sing, D. H. Everett, R. A. W. Haul, L. Moscou, R. A. Pierotti, J. Rouquerol, T. Siemieniewska, *Pure. Appl. Chem.* **57** (1985) 603
35. S. Lowell, J. E. Shields, M. A. Thomas, M. Thommes, *Charactrization of Porous Solids and Powders: Surface Area, Pore Size and Density*, Kluwer Academic Publishers, Dordrecht, 2004, p. 44 (ISBN 978-1-4020-2303-3)
36. K. Hatakeyama, M. Okuda, T. Kuki, T. Esaka, *Mater. Res. Bull.* **47** (2012) 4478 (https://doi.org/10.1016/j.materresbull.2012.09.057)
37. L. Luo, Y. Li, J. Hou, Y. Yang, *Appl. Surf. Sci.* **319** (2014) 332 (https://doi.org/10.1016/j.apsusc.2014.04.154).